inter.noise 2014
MELBOURNE AUSTRALIA
16-19 NOVEMBER

Results of the ray-tracing based solver BEAM for the approximate determination of acoustic backscattering from thin-walled objects

Ralf BURGSCHWEIGER[1]; Ingo SCHÄFER[2]; Martin OCHMANN[1]; Bodo NOLTE[2]

[1] Beuth Hochschule für Technik Berlin, Research Group Computational Acoustics, Berlin, Germany

[2] Federal Armed Forces Underwater Acoustics and Marine Geophysics Research Institute (WTD71/FWG), Kiel, Germany

ABSTRACT

The calculation of the acoustic backscattering from larger thin-walled underwater objects requires, especially in the middle and higher frequency range, computing resources that are usually not available in practice. Therefore, the use of appropriate approximate methods appear useful for those cases.

In this paper, a solution method is presented that is tracking "sound beams", generated by a plane wave and impinging on a submerged object. The method determines the complex reflection and transmission coefficients at the incident points, taking into account shell boundary conditions, and generates “child”-beams which are then followed up to a predefined level. Therefore, the material-dependent refraction and a possible multiple reflection can be considered within the structure. An appropriate post-processing calculation provides the backscattered sound pressure in the far field.

Results for "inner" structures that include reflective areas and which are surrounded by thin “outer” shell structures are presented and compared with results of FEM-based applications (where applicable). Additionally, a method to determine the "hot spots" based on monostatic calculations is described.

Keywords: Numerical Methods, Underwater Acoustics, Ray Tracing, Backscattering
I-INCE Classification of Subjects Number(s): 75.4, 75.5, 75.9, 76.4

1. INTRODUCTION AND BASICS

To calculate the frequency-dependent acoustic backscattering of an object, especially for coupled cases, time consuming numerical methods (FEM / BEM) must be used. In these methods, the computational effort increases strongly with the excitation frequency, since the required discretization of the surface(s) and/or the volume(s) must be performed correspondingly fine.

The classic rule of thumb for determining the element size requires at least six elements per wave-length when using BE methods. This problem can be reduced with the help of high-frequency approximation methods (PWA, Kirchhoff-Approximation). Within these methods, optical analogies are used, which are only allowed for large frequencies.

1.1 Acoustic Backscattering

The acoustic sound backscattering of the surface Γ of the object can be calculated by means of the Kirchhoff-Helmholtz integral (Eq. 1) at a known pressure and velocity field on the surface (with the function g as the fundamental solution of the Helmholtz equation).

$$p_{scat} = \int_{\Gamma} \left[g\,\frac{\partial p}{\partial n} - p\,\frac{\partial g}{\partial n} \right] d\Gamma \tag{1}$$

With the use of a full coupled boundary element calculation, the unknown pressure and the velocity values could be determined on the surface Γ of the object and then, in a post-processing step, the backscattered sound pressure at any point in the far field, too.

1 burgi@beuth-hochschule.de; ochmann@beuth-hochschule.de
2 ingo5schaefer@bundeswehr.org; bodonolte@bundeswehr.org

1.2 Ray-tracing based approach

The numerical method for coupled problems mentioned above requires a very high computational effort, especially at high frequencies. This can be significantly reduced if the unknown pressure and velocity values on the surface can be determined by means of ray-theoretical approaches.

$$p^R = Rp^i \, , \, p^T = Tp^i \tag{2}$$

Here, the incident sound beam p^i leads to a reflected p^R and a transmitted p^T sound beam. The reflection coefficient R and the transmission coefficient T (Eq. 2) can be calculated by means of the methods specified by Brekhovskikh (1).

This method is based on the assumption that the law of reflection for plane waves on infinite plates is applied for each sound beam. For this reason, the method is suitable for high frequencies.

1.3 Beam path tracing

The beam path to track can be explained using an example consisting of a rigid angle inside a thin-walled sphere (Figure 1, Figure 2).

The incident beam (0, red) hits the thin spherical shell and is divided into two beams. The first reflected beam (1R, blue) leaves the structure and hits no other surfaces. The transmitted beam (1T, green) runs inside, finds the top corner and is tracked until it leaves the structure (5T, blue).

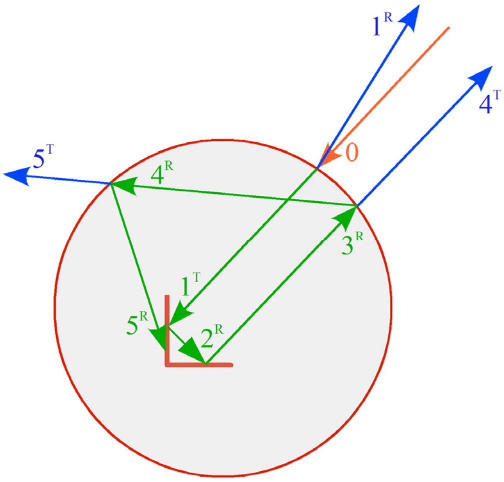

Figure 1 - 2D ray tracing (maximum level 5)

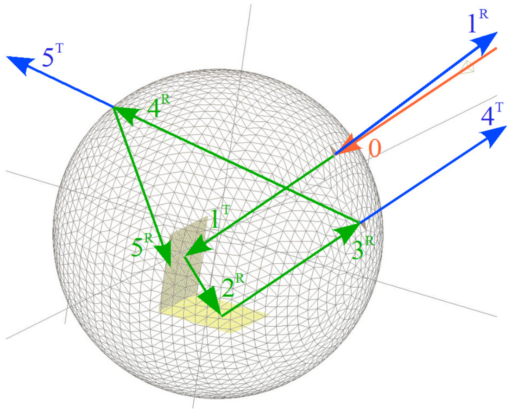

Figure 2 - 3D ray tracing (maximum level 5)

The Kirchhoff-Helmholtz integral (Eq. 1) for determining the acoustic sound backscattering is now performed only on the integration area for all out-going N beams (Figure 1, 2, blue rays).

The incident plane wave is described according to Figure 3 by a number of equal sized beams.

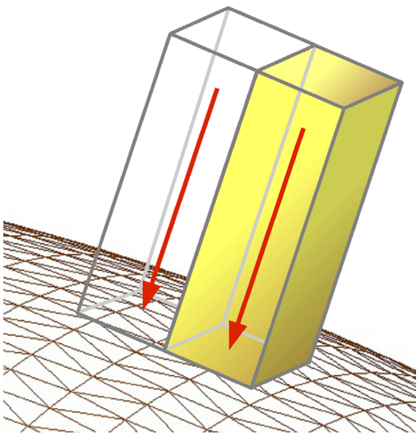

Figure 3 - Relevant area of a beam with a fixed size

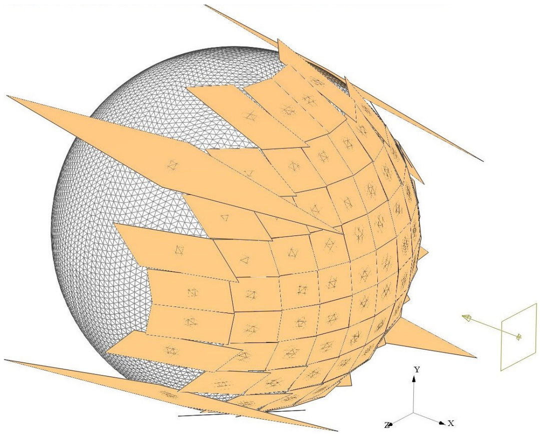

Figure 4 - Projected surface using a fixed beam size

The surface of a sphere e.g. is therefore not precisely modeled, but simulated by the projection of these beams (Figure 4).

1.4 Fast hit algorithm

To be able to perform the ray tracing, the surface element hit by the beam must be determined. This can be very time consuming for large numbers of elements in complex structures. For this reason, the elements of the object are placed within boxes which are enclosed by spheres. Then, each box is recursively divided into eight sub-boxes (“octants”).

To determine which element will eventually be hit by the beam, it is first checked if there is an intersection with the box at level 1. When struck, all boxes at level 2 will be examined. This continues recursively until the box with the highest available level is reached. Figure 5 gives a 2D example for a beam hitting an element in a box at box level 6.

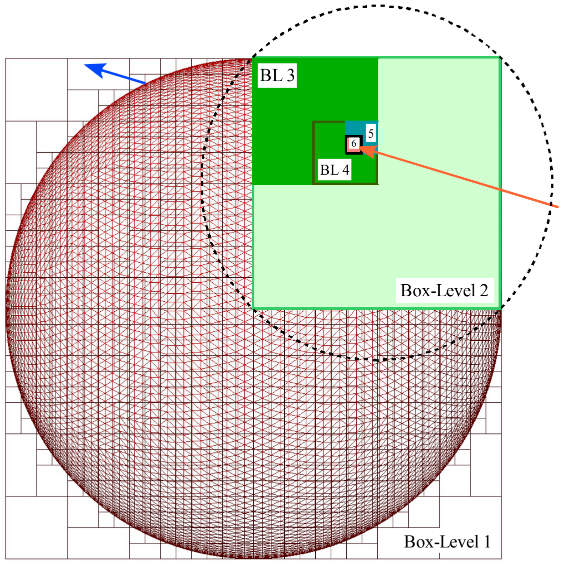

Figure 5 - Boxing structure (2D)

Table 1 - Level-specific elements per box relationship

Level L_{box}	Elements $N_{max,elem/box}$	Boxes $N_{box/L}$
1	1.000.000	1
2	125.000	8
3	15.625	64
4	1.953	512
5	244	4.096
6	30	32.768
7	4	262.144

Table 1 shows the number of elements that are in one box, depending on its level. The box at level 7 contains e.g. a maximum of four elements, which are then individually tested for a hit. In this manner the element can therefore be found with a very small number of comparisons.

This “Hit check” algorithm is based on the boxing algorithm used within the Multi-Level Fast Multipole Method (MLFMM) published in (2).

1.5 Optimizations

1.5.1 Parallelizability

The BEAM method can be parallelized well when subsets of the required "start beams” are assigned to the available CPU cores, since the tracing of a single beam is independent of all others.

However, the reduction of the solution time can not be completely proportionally scaled because the numbers of transmitted or reflected "child beams" may vary and thus one can not achieve a 100% CPU usage. Table 2 shows an example of the thread-depending solution times of the process.

Table 2 - Solution times for different thread counts

Number of threads N_{thread}	Beams per thread $N_{b/t}$	Solution time $\Delta t_{tot,conv}$
1	2,920	12.090 s
2	1,460	6.506 s
4	730	3.510 s
8	365	2.012 s
16	183	1.139 s
20	146	0.967 s

1.5.2 Monostatic frequency sweeps

Often the monostatic scattering of the object must be determined, where the sound source is positioned at each evaluation point ("field point").

Usually, an outer loop over the frequency range and an inner loop over the field points is performed. Thus, the total time $\Delta t_{tot,conv.}$ is linearly dependent on the sum of the computational time per frequency Δt_f and per field point Δt_{src}, on the number of frequencies N_f and of field points N_{fp} (Eq. 3):

$$\Delta t_{tot,conv} \approx (\Delta t_{src} + \Delta t_f) \times N_f \times N_{fp} \tag{3}$$

However, for the BEAM process it is useful to change the order so that the outer loop runs over the field points and the inner loop over the frequencies. All geometric (field point specific) calculations (Δt_{src}) are independent of the current frequency and must be done only once per frequency step (outer loop). For the following frequency values only the calculation of transmission and reflection components (requiring Δt_f) must be performed per field point and can be carried out within the inner frequency loop (Eq. 4):

$$\Delta t_{tot,opt} \approx (\Delta t_{src} + \Delta t_f) \times N_f \quad + \quad (\Delta t_f \times (N_{fp} - 1)) \tag{4}$$

This allows the reduction of the computation time starting at the second frequency (for a total of 21 frequencies) to about $^1/_{20}$ of the value of the first calculation (Table 3).

Table 3 - Example for the reduction of the solving times for monostatic frequency sweeps

Number of frequencies N_f	Solving time $\Delta t_{tot,conv}$ (conv.)	Solving time $\Delta t_{tot,opt}$ (opt.)	Time per freq. $\Delta t_{f,opt}$ (opt.)
1	198 s	198 s	198 s
2	396 s	209 s	105 s
21	8,320 s	401 s	19 s

2. RESULTS

In this paper the results of the BEAM method are presented for thin-walled structures. Details, results and computing times for rigid calculations can be found in (3).Within all calculations, water was used as the surrounding fluid.

2.1 Example 1: Simple cone, sound impinging on the cone end

A simple thin shell cone with an apex angle of 90° and a radius and length of 1 m is used as the first example (Figure 6). A plane wave is impinging on the cone end in positive X direction (green arrows in Figure 6 and 7). The evaluation points are placed on a circle in the XY-plane, using a distance of 10 km, and the resulting pressure in the far field is calculated back to a distance of 1 m to the center, giving the normalized pressure level $L_{p,n}$ in [dB] (blue curves).

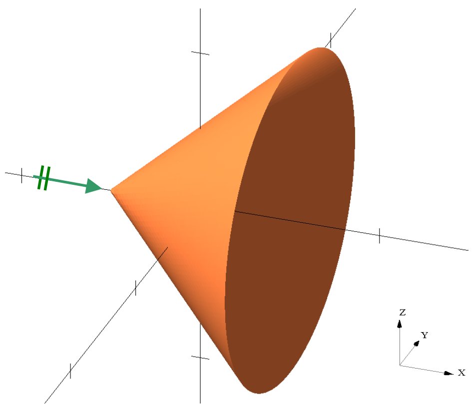

Figure 6 - Cone with an apex angle of 90°, plane wave in positive X direction

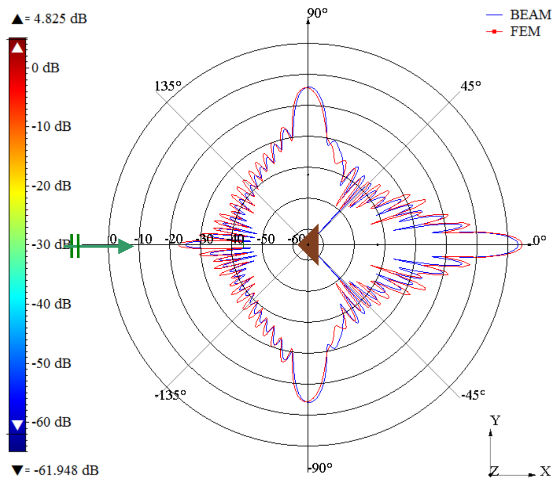

Figure 7 - normalized pressure level (polar plot). shell cone, f = 10 kHz, steel, 1 mm

This example allows the comparison with results obtained from a FEM based application (COMSOL, red curves), using the rotation-symmetric 2D case to reduce the FEM computation times.

In the following the results will be always displayed as a curve over the evaluation angle in order to illustrate the quantitative differences.

Case 2.1.a: Steel, 1 mm (Figure 8)

The maxima at ±90° and in the “shadow” at 0° are clearly visible, the monostatic value (here at 180°) is around -23 ... - 26 dB. The quantitative differences between both methods for the 1 mm steel shell are less than 3 dB, with regard to the maxima they are less than ±1 dB.

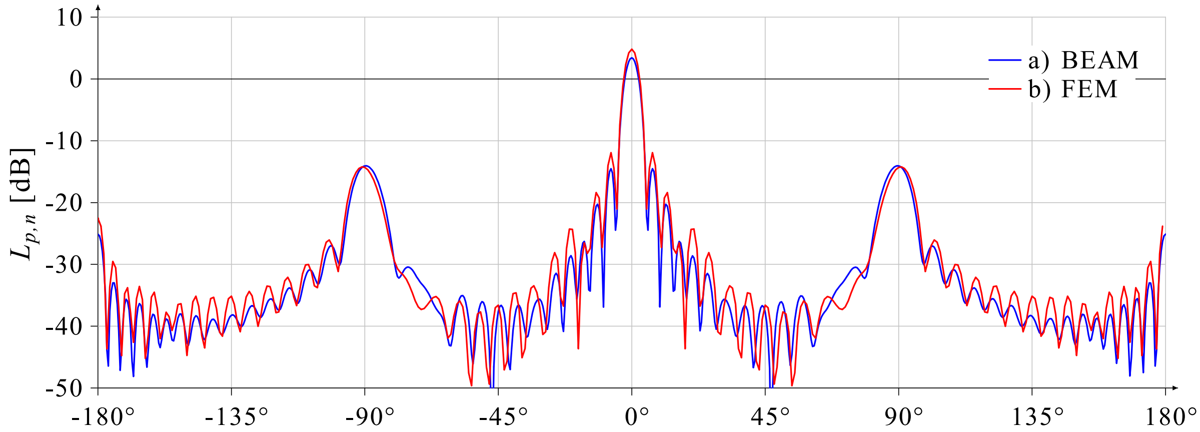

Figure 8 - normalized pressure level of the shell cone at f = 10 kHz, steel, 1 mm

Case 2.1.b: Steel, 2 mm (Figure 9)

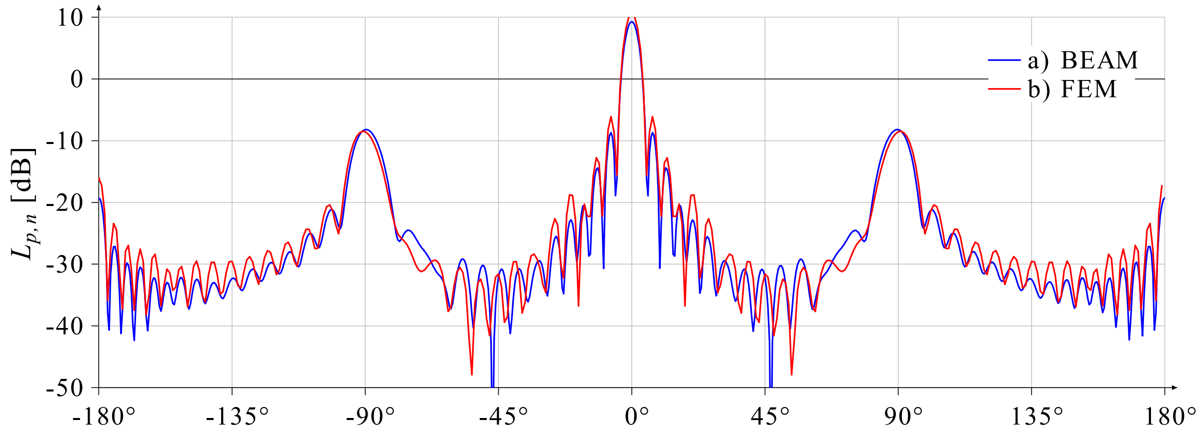

Figure 9 - normalized pressure level of the shell cone at f = 10 kHz, steel, 2 mm

The quantitative differences are still very small.

Case 2.1.c: Steel, 10 mm (Figure 10)

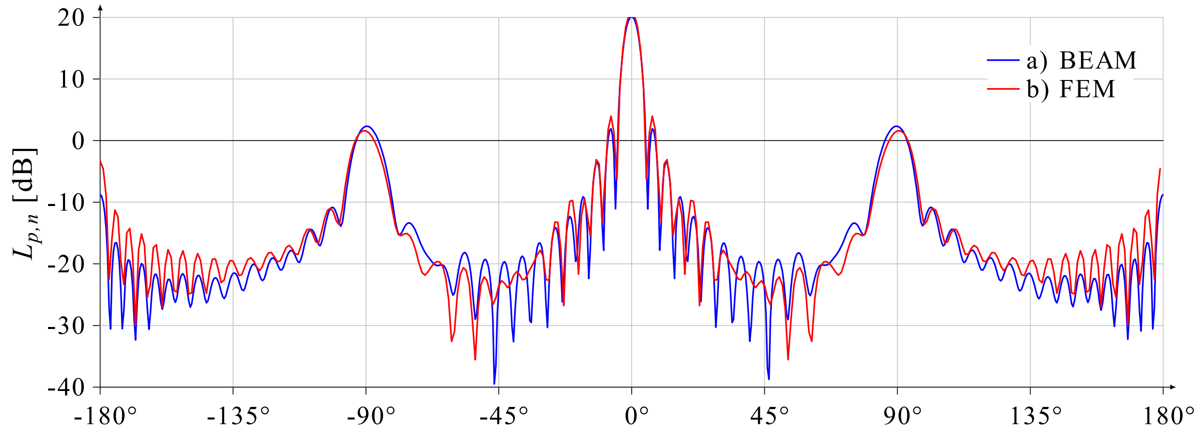

Figure 10 - normalized pressure level of the shell cone at f = 10 kHz, steel, 10 mm

The differences at the maxima are still very small, but in the “quieter” regions (below -10 dB) first differences of up to 10 dB are coming up.

2.2 Simple cone, steel, sound impinging into the cone opening

Now the plane wave is impinging into the cone opening in negative X direction (green arrows, Figure 11 and 12). The main difference compared to the sound source impinging on the cone end is the higher monostatic reflection (here at 0°, Figure 12) of -11 (FEM) ... -15 dB (BEM) due to the mirror-like reflection in the cone, while the other maximum values are nearly equal.

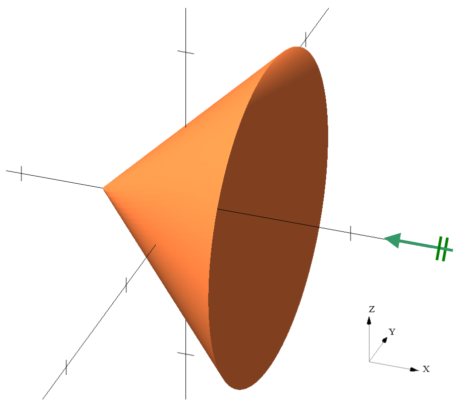

Figure 11 - Cone with an apex angle of 90°, plane wave in negative X direction

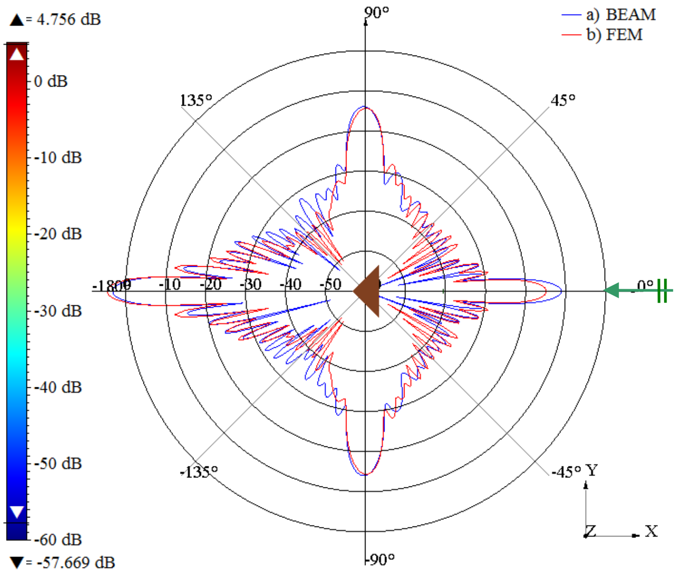

Figure 12 - normalized pressure level (polar plot). shell cone, f = 10 kHz, steel, 1 mm

Case 2.2.a: Steel, 1 mm (Figure 13)

Figure 13 shows the values over the elevation angle. Please note that these angle-dependent values are "shifted" by 180° due to the change of the plane wave direction when looking at the previous results (cases 2.1.a ... 2.1.c).

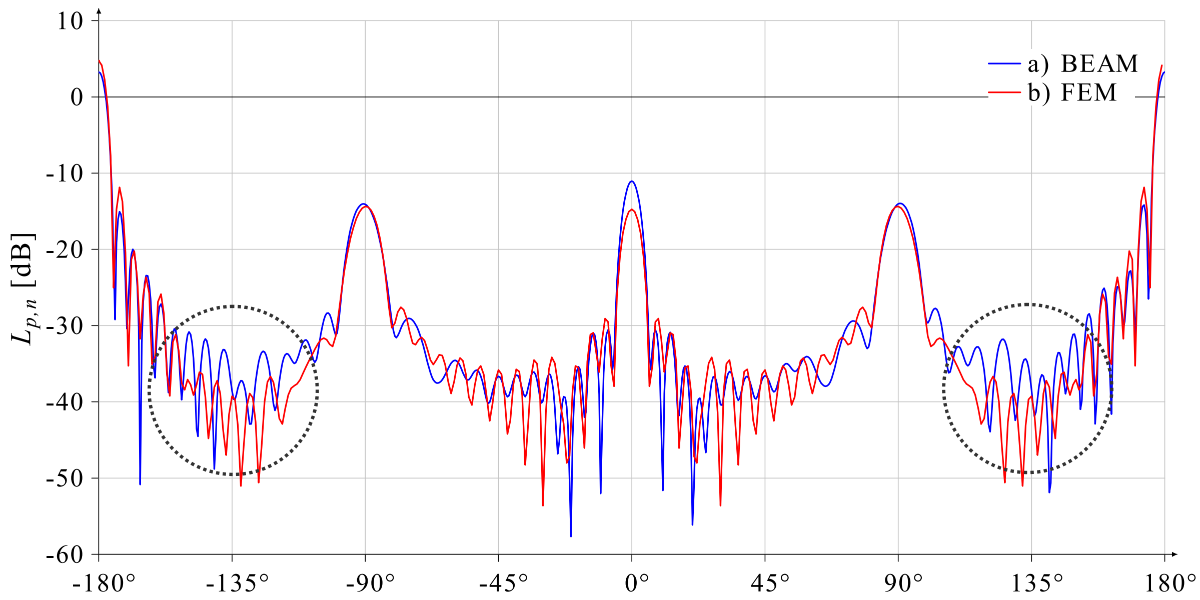

Figure 13 - normalized pressure level of the shell cone at f = 10 kHz, steel, 1 mm

The quantitative differences between both methods for the 1 mm steel shell are small at the maxima (less than 4 dB), only where the levels become below -30 dB, some bigger differences can be found (dotted circles).

Case 2.2.b: Steel, 10 mm (Figure 14)

The level at the monostatic evaluation point (0°) grows with the thickness of the shell due to the fact, that the problem approaches the “rigid” case (green graph).

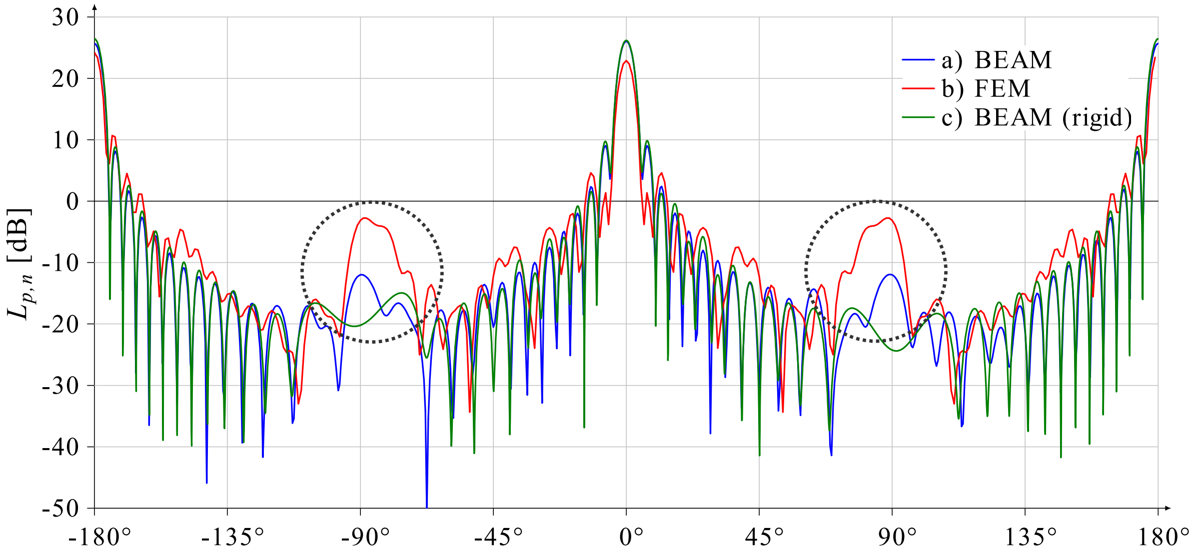

Figure 14 - normalized pressure level of the shell cone at f = 10 kHz, steel, 10 mm

While all pressure level values are increasing with regard to the thickness of the shell, the quantitative differences between the FEM and the BEAM solution are still at about max. 4 dB in the level range above -20 dB, except at ±90° (dotted circles), where the values of the FEM result are about 10 dB higher due to the fact, that the BEAM method is not able to consider the diffraction at the edge of the cone.

2.3 Example 2: Cone within a sphere

A rigid cone with a radius and length of 1 m is placed in a steel shell sphere with a radius of 1.5 m and 20 mm thickness (Figure 15). Water is used for the inside and the outside fluid.

The structures are hit by a plane wave in negative x-direction (green arrow). The normalized backscattered pressure level $L_{p,n}$ is evaluated in the far field at a monostatic field point (x_{FP} = 10 km, y_{FP} = 0 m, z_{FP} = 0 m).

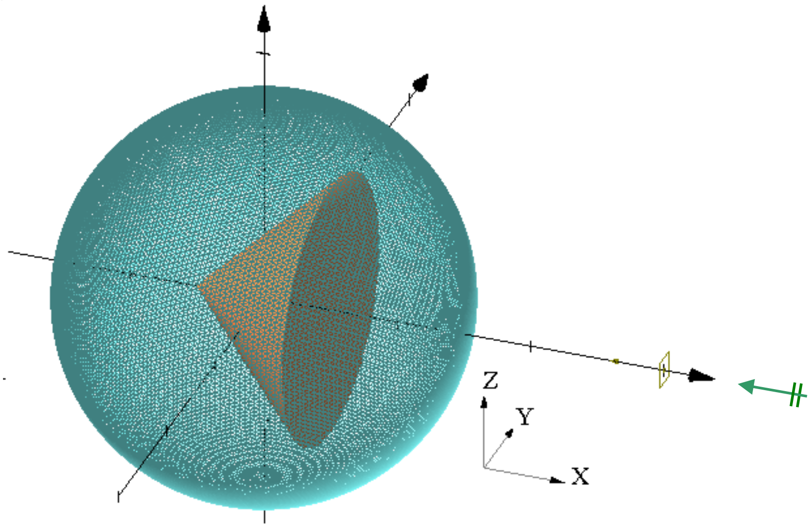

Figure 15 - Cone with steel shell

At low frequencies, it is expected that the influence of the rigid cone is visible, while with increasing frequency the outer shell dominates and the normalized pressure level will converge against the analytic value for a rigid sphere (r = 1.5 m, f = 10 kHz) in water of approx. -2.5 dB.

The result of the BEAM method (Figure 16, green curve) can be compared with a FEM based solution (magenta curve). Additionally, the results for a rigid cone only (blue curve) and a rigid sphere (orange curve) with the same size as the steel shell are shown.

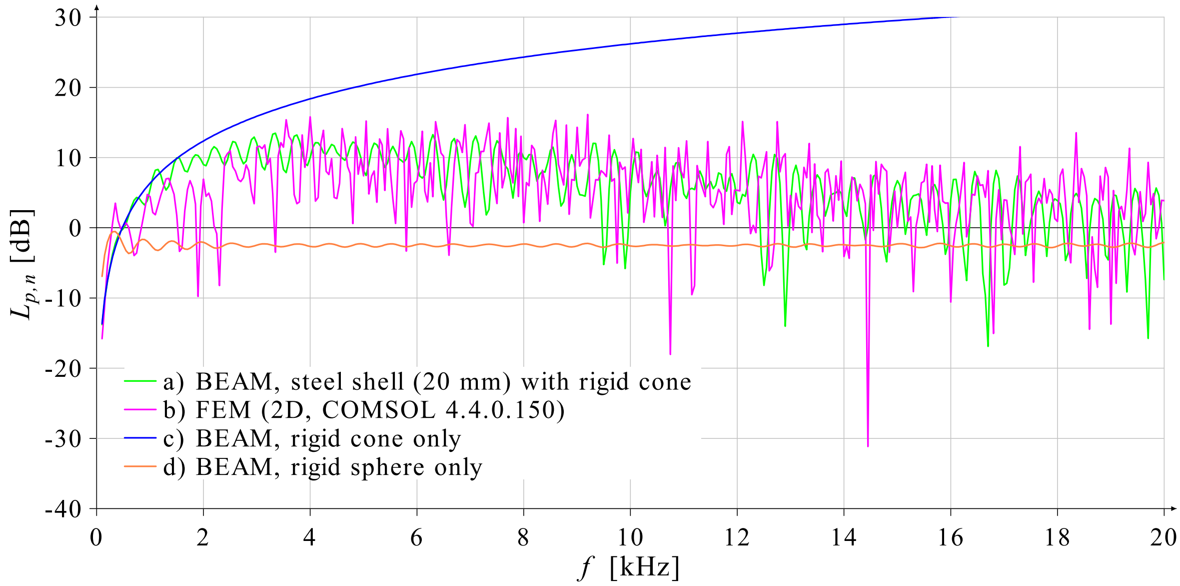

Figure 16 - normalized pressure level of the cone with a shell sphere (steel, 20 mm) at the monostatic field point [10 km; 0 m; 0m], frequency range: 0 ... 20 kHz

Although both curves are oscillating heavily, still a certain quantitative average agreement can be seen, even the expected approach to the respective rigid equivalents.

Obviously, both methods seems to be very sensitive to small changes in frequency and geometry, so it is not easy to compare both solutions with regard to quality and quantity.

2.4 Example 3: Complex model of a round cylinder with triple mirrors and a conical shell

To illustrate the advanced capabilities of the BEAM method, a rounded cylinder is used with several triple mirrors on the caps. The cylinder is surrounded by a conical shell (Figure 17, approx. size 49 × 10 × 10 m). This model is one case of the BeTSSI-II workshop presented in (4).

The inner cylinder and the triple mirrors (“cat-eyes”) at the left end are represented by steel with a thickness of 2 cm and filled with air. The outer conical hull is made of steel with a thickness of 8 mm, filled with and surrounded by water.

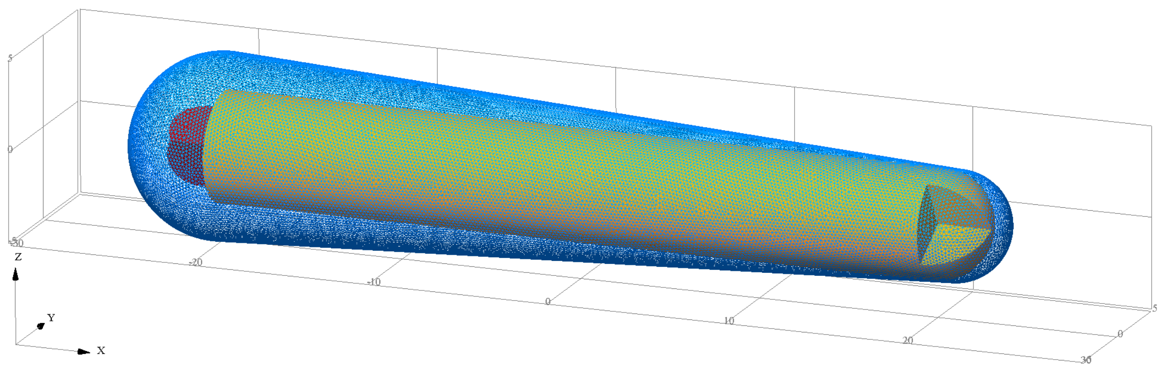

Figure 17 - Complex model of a round cylinder with one resp. four triple mirrors at the ends, surrounded by a conical rounded shell

A grid in the form of a spherical segment (longitude λ_L of -180 ... +180°, latitude φ_B of -20 ... +20°, using angular steps of 0.5°) is placed in the far field at a distance of 10 km around the object.

Its nodes are used as evaluation points (total 58,401 points) for a monostatic calculation, that means, the position of the sound source was moved to each evaluation point. For a better representation of the results, a projection distance of 30 m is used (Figure 18). The size and complexity of this model makes a monostatic calculation with BE or FE methods in a realistic time almost impossible, and is feasible only with the use of the BEAM method.

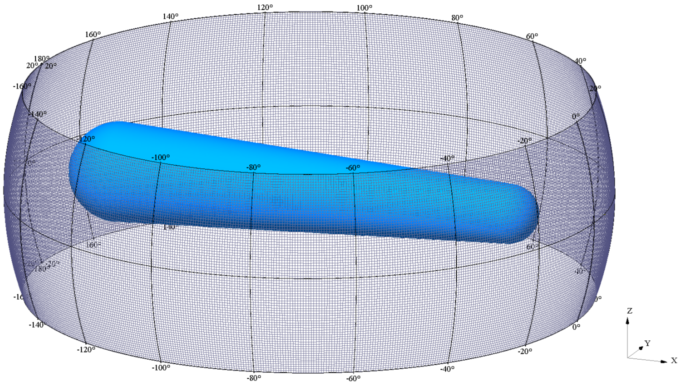

Figure 18 - Spherical evaluation surface (58,401 nodes), using a projection distance of 30 m

The normalized sound pressure level $L_{p,n}$ was calculated for a total of 21 frequencies (f = 8 ... 12 kHz, step width Δf = 0.1 kHz) for all 58,401 evaluation points, in addition an appropriate averaging process was carried out over all frequencies used (Figure 19).

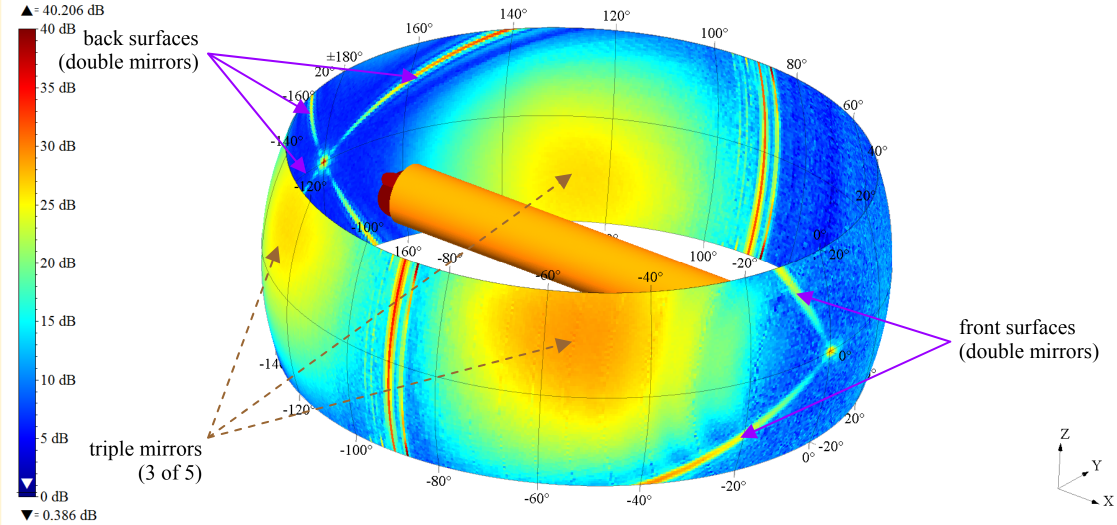

Figure 19 - averaged normalized pressure level $L_{p,n}$ for f_{aver} = 10 kHz

One can clearly see the effects of the triple mirrors in the front and rear (brown dashed arrows), as well as the double reflections at these parts (purple arrows).

The advantage of averaging over the frequencies in comparison with a single frequency solution (Figure 20) having strong interference patterns is clearly visible.

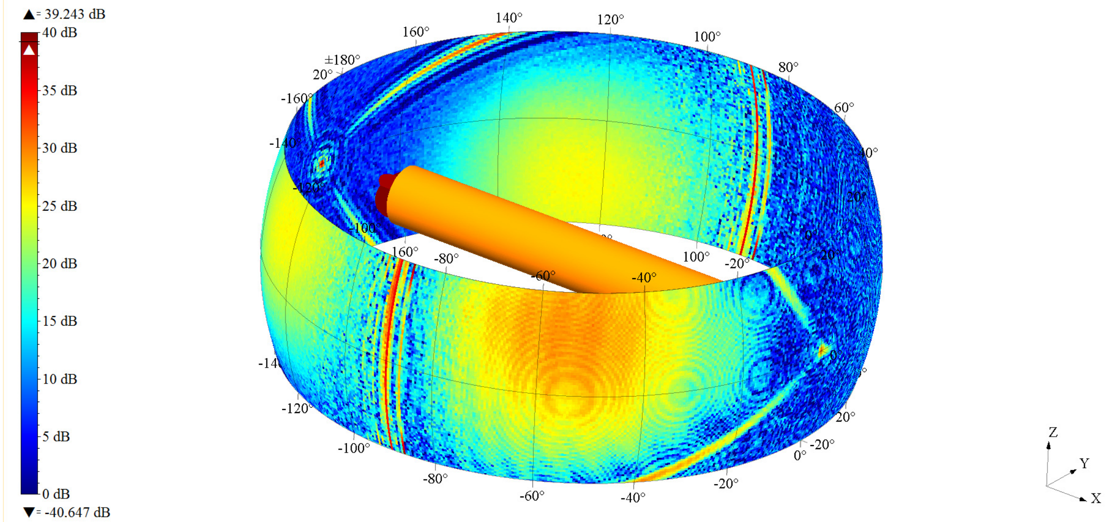

Figure 20 - normalized pressure level $L_{p,n}$ for f = 8 kHz, color range adapted to 0 ... 40 dB

The computation time for all 58,401 evaluation points and all 21 frequencies was about 6,976 s on a 20 core workstation, which corresponds to a mean solving time of 0.119 s per point.

Figure 21 shows the planar projection of the pressure as a 2D representation.

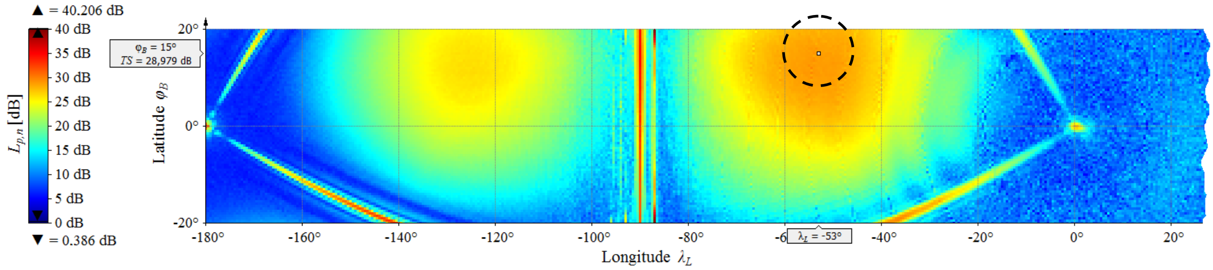

Figure 21 - planar projection of averaged normalized pressure level $L_{p,n}$ for f_{aver} = 10 kHz

Here, a so-called "analyzer" allows the selection of hotspots by specifying a longitude (here: λ_L = -53°) and a latitude (here: φ_B = 15°) angle. Then, a separate calculation can be performed providing the corresponding pressure distribution on the basis of an integration over all the beams in the far field.

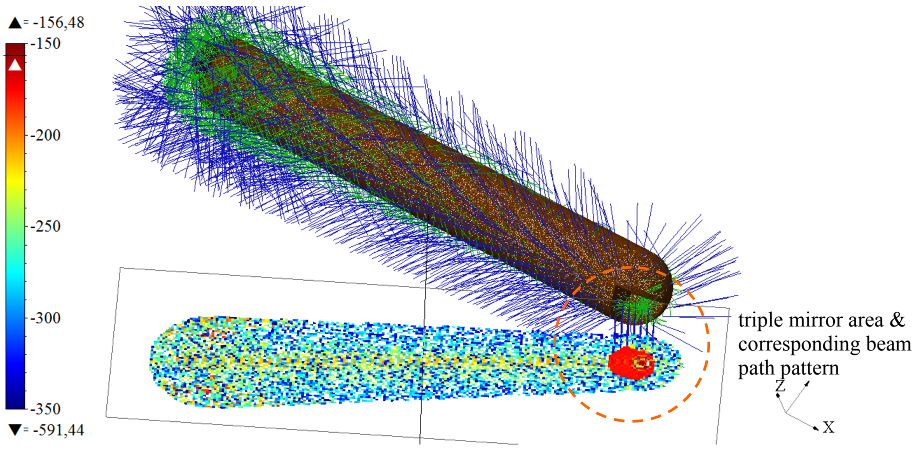

Figure 22 - Result of the "analyzer" at λ_L = -53° and φ_B = 15° (with beam path pattern)

The maxima at this point which results from the triple mirror at the front of the inner cylinder can be clearly identified. It is also possible to visualize the corresponding beam path pattern.

3. CONCLUSIONS

The obtained results show the good agreement between the approximate BEAM method and the FE method for coupled problems with thin shells where applicable.

The results of both methods for the calculation of frequency sweeps are still extremely sensitive to small changes in frequency and material parameters, here further investigations and appropriate improvements are still necessary.

The primary advantage of the BEAM method is the high computational speed, especially in monostatic calculations for multiple frequencies, and the ability to take into account regions of multiple reflections. However, the method can only be used for computations in the far field, because it does not provide surface-specific values.

The analysis function described also needs further development in order to represent the complete beam path for a selected point in detail, for example.

REFERENCES

1. Brekhovskikh L. M.: "Waves in Layered Media", Academic Press, New York, 1960.
2. Burgschweiger R., Schäfer I. und Ochmann M.: "A Multi-Level Fast Multipole Algorithm (MLFMM) for calculating the Sound scattered from Objects within Fluids", Proceedings of ICA 2010, Sydney, Australia.
3. Burgschweiger R., Schäfer I., Ochmann M. and Nolte B.: "BEAM: A ray-tracing based solver for the approximate determination of acoustic backscattering of thin-walled objects - Basics and Implementation", Proceedings of Forum Acusticum 2014, Krakow, Poland.
4. Nolte B., Schäfer I., de Jong C. and Gilroy L., "BeTSSi II Benchmark on Target Strength Simulation", Proceedings of Forum Acusticum 2014, Krakow, Poland.